

# SPOTS: An Accelerator for Sparse CNNs Leveraging General Matrix-Matrix Multiplication

Rutgers Department of Computer Science Technical Report: DCS-TR-756

Mohammadreza Soltaniyeh<sup>§\*</sup> Richard P. Martin<sup>§‡</sup> Santosh Nagarakatte<sup>§\*</sup>

<sup>§</sup>Department of Computer Science, Rutgers University, \*m.soltaniyeh,santosh.nagarakatte@cs.rutgers.edu

<sup>‡</sup>rmartin@scarletmail.rutgers.edu

**Abstract**—This paper proposes a new hardware accelerator for sparse convolutional neural networks (CNNs) by building a hardware unit to perform the Image to Column (IM2COL) transformation of the input feature map coupled with a systolic array-based general matrix-matrix multiplication (GEMM) unit. Our design carefully overlaps the IM2COL transformation with the GEMM computation to maximize parallelism. We propose a novel design for the IM2COL unit that uses a set of distributed local memories connected by a ring network, which improves energy efficiency and latency by streaming the input feature map only once. We propose a tall systolic array for the GEMM unit while also providing the ability to organize it as multiple small GEMM units, which enables our design to handle a wide range of CNNs and their parameters. Further, our design improves performance by effectively mapping the sparse data to the hardware units by utilizing sparsity in both input feature maps and weights. Our prototype, SPOTS, is on average 1.74× faster than Eyeriss. It is also 78×, and 12× more energy-efficient when compared to CPU and GPU implementations, respectively.

## I. INTRODUCTION

Technology trends have driven the ability of neural networks to solve a wide variety of problems in video processing [26], speech recognition [13], and natural language processing [19], [44]. The spectrum of designs to realize neural network abstractions is vast, ranging from the general-purpose, *i.e.*, CPUs, to GPUs and FPGAs [34], to specialized systolic arrays [24], all the way to entirely analog circuit implementations [40].

Among various neural networks, Convolutional Neural Networks (CNNs) have unique features that make building architecture-specific accelerators challenging, as well as opening opportunities for improvement. In particular, all CNNs have common design patterns that can be exploited to improve performance and energy efficiency over more general-purpose designs. CNNs use distinct neural layer types, including convolution, fully connected, and pooling, although the bulk of the computation resides in the convolutional layers. These common layer types thus present the opportunity to build specialized accelerators general to all CNNs. This paper proposes a novel architecture, SPOTS, to specifically improve performance and energy efficiency of CNNs for inference tasks.

One approach to implement CNNs is to realize a convolutional layer as a large, single General Matrix-Matrix Multiplication (GEMM) using a data reorganization transformation called Image-to-Column (IM2COL). We found that the IM2COL extra step, on average, contributes to 29% of the overall execution

time on CPUs. A convolution operation can be defined as sliding a smaller filter window over a large array with a stride size, producing patches (see Figure 1 and Figure 2(b)). Many elements are shared between the patches. Hence, IM2COL performs many redundant accesses.

Our accelerator, SPOTS, includes a dedicated hardware IM2COL unit that operates in parallel with the hardware GEMM unit. A novel aspect of the IM2COL unit in SPOTS is that it has a collection of patch units that streams the input only once, performs data reorganization, creates multiple patches in parallel, and eliminates redundant accesses. These patches are subsequently fed into a systolic array based GEMM unit.

Convolution layers vary in their number of filters, kernel size, stride values, and feature map dimensions. These variations result in matrices with different characteristics that make it challenging to obtain high utilization on square systolic arrays. A rigid structure of systolic array processing elements (PEs) can be under-utilized for specific matrix shapes and sizes. Further, certain designs are tailored to the needs of the convolution layers and can underperform for other computations, such as fully-connected layers [11], [37].

The systolic array in SPOTS is novel in that it has a *tall-thin* shape, which allows for significant overlap of the PEs performing the matrix multiplication with the PUs executing the IM2COL reorganization. However, a drawback of tall-thin shapes is that the PEs are under-utilized for layers with a small number of filters. We enhance our design to provide the ability to organize it as multiple small GEMM units, which achieves high PE utilization for a wide range of CNNs. In addition to the convolution and fully connected layers, SPOTS support pooling layers with a minor enhancement to the IM2COL unit.

Pruning is a neural network technique to reduce computation and memory footprint by eliminating weights after the training phase without substantively changing network accuracy. Pruning results in sparser arrays; that is, portions of the array have many zero elements. SPOTS is thus sparsity aware, to take advantage of the opportunity to skip data transfer and computation for sparse regions. The sparse format, based on group-wise pruning, substantially reduces the memory footprint of the weights in comparison to random pruning techniques [17]. Finally, SPOTS tags blocks of zeros in the result of the IM2COL unit and skips zero elements before entering the systolic array, saving computation cycles and memory transfers.

The three main innovations in our accelerator are: (1) a novel

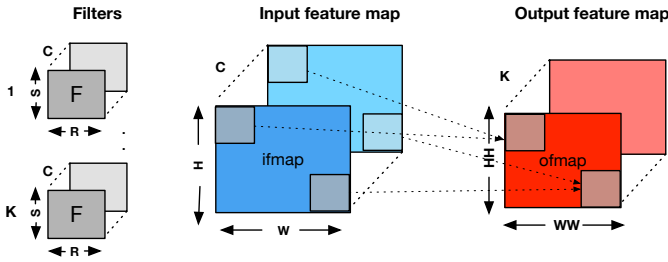


Fig. 1: Illustration of a convolution layer along with its inputs.

IM2COL unit that allows it to pipeline GEMM and IM2COL computations to improve performance, (2) a tall-thin array for GEMM with the capability to adapt to different CNN layers and shapes, and (3) sparsity awareness that allows the design to exploit the sparsity in both the feature map and filters. These techniques combine to improve CNN performance and energy efficiency over prior accelerators. Our results show SPOTS can achieve  $1.7\times$  speedup over prior work. It is  $78\times$  and  $12\times$  more energy efficiency when compared to CPU and GPU systems, respectively. Our evaluations demonstrate high PE utilization under different CNN shapes.

## II. BACKGROUND AND MOTIVATION

We provide background on CNNs, structuring the convolution operation as general matrix-matrix multiplication with the help of the IM2COL transformation, and leveraging sparsity in the weights to improve performance and energy efficiency.

**CNNs.** A Convolution Neural Network (CNN) consists of a series of layers. Each layer in a CNN extracts a high-level feature of the input data called a *feature map* (fmap). CNNs often have different layers, including convolution, activation (e.g., non-linear operator), pooling, and fully connected layers. The convolutional layers are the main layers in a CNN. They perform the bulk of the computation. Each convolution layer has several filters. The values of these filters (i.e., weights) are learned during the training phase. In the inference phase, which is the focus of this paper, the network classifies new inputs presented to the network.

Figure 1 visualizes the computation in the convolution layer. The input feature map is structured as a 3-D tensor with  $W$ ,  $H$ , and  $C$  as its width, height, and the number of channels, respectively. Similarly, the filters are structured as 3-D tensors with width ( $R$ ), height ( $S$ ), and  $C$  channels. The filters and the input feature maps have the same number of channels. There are  $K$  filters in this example. Typically, a collection of  $N$  input feature maps are convolved with  $K$  filters (i.e., a batch size of  $N$ ). For inference tasks, it is common to use a batch size of 1. For some convolution layers, a 1-D scalar bias is also added to the result, which is not shown in Figure 1.

**Transforming convolution to general matrix-matrix multiplication.** The convolution operation can be transformed into a general matrix-matrix multiplication (GEMM) using the IM2COL transformation. To structure the convolution operation as matrix multiplication, we need to create two matrices from

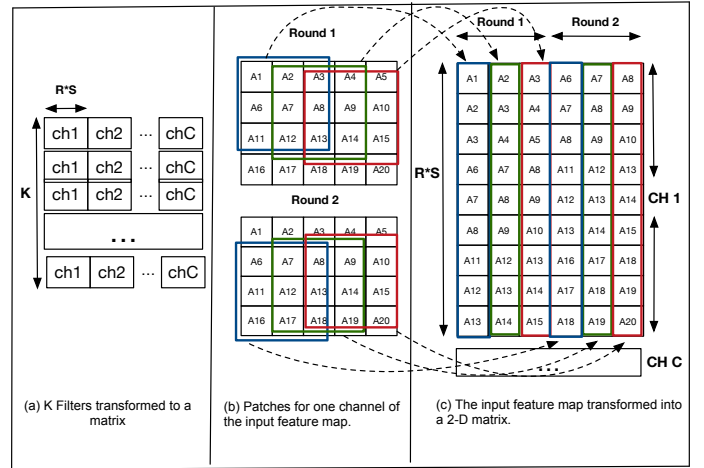


Fig. 2: Transforming the inputs of a convolution layer (i.e., input feature map and filters) into two matrices to use a GEMM-based formulation of convolution.

the two inputs of a convolution layer: input feature map and the  $K$  filters.

Figure 2 illustrates how the two matrices are built. The product of these two matrices will be equivalent to the result of the convolution operation.

For building the weight matrix, each filter is mapped to one row of the weight matrix. When there are  $K$  filters, there will be  $K$  rows in the weight matrix (see Figure 2(a)). The number of columns in the weight matrix is  $R \times S \times C$ . In contrast to the weight matrix, a more complex transformation is required to build a 2-D matrix from the original 3-D input feature map. This transformation is called **Image to Column (IM2COL)**. The IM2COL result depends on the kernel size and the stride size, which are the two parameters of the convolution operation. In convolution, each filter slides across different positions in the input feature map. We call all elements in the input feature map covered by the filter as a *patch*. Patches are often overlapped with each other when the stride size is less than filter size. This overlap results in the repetition of the same element of the input feature map in multiple patches. Figure 2(b) and Figure 2(c) illustrates the IM2COL transformation with an example filter of size  $(3 \times 3 \times C)$  and a stride of 1. Each column of the matrix produced by the IM2COL transformation corresponds to one patch where the filter is applied, and it has  $R \times S \times C$  rows. Figure 2 shows the patches for one channel. Finally, the product of the two matrices (Figure 2(a) and 2(c)) generates the output of the convolution operation.

**Why a GEMM-based convolution operation?** GEMM is a core building block in many software frameworks and ASICs [1], [24]. The design space of GEMM operations can be carefully explored to improve performance. Further, fully connected networks and other neural networks (e.g., Long Short Term Memory (LSTM) and Graph Convolution Networks (GCN)) can be structured as a GEMM operation. Hence, optimizing a general building block such as GEMM can result

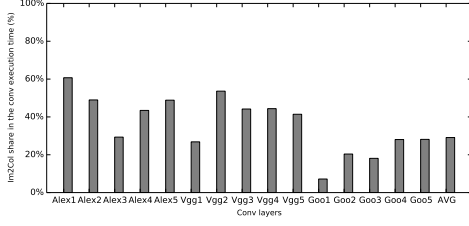


Fig. 3: The percentage of the total execution time spent in the IM2COL transformation for various convolution layers from AlexNet, VGGNet, and GoogleNet.

in good performance not only for convolution operations but also other operations (e.g., fully connected layers) [11], [37]. A key to a GEMM-based formulation of convolution is the IM2COL transformation that enables IM2COL and GEMM operations to be optimized separately. Many widely used frameworks such as Caffe and PyTorch use a GEMM-based formulation of convolution to utilize highly optimized libraries for CPUs and GPUs.

**Challenges with a GEMM-based formulation.** Although GEMM-based convolution is widely used; there are two main challenges in attaining good performance and energy efficiency using such a formulation. First, the IM2COL transformation creates extra computation. The total execution time for the IM2COL transformation can be as high as 60% of the total execution for the convolution operation. Figure 3 reports the percentage of the total execution time that is spent in the IM2COL transformation for various layers in AlexNet, VGGNet, and GoogleNet. On average, the IM2COL transformation spends 29% of the overall execution time while using the Caffe framework for running three CNN networks: AlexNet, VGGNet, and GoogleNet. Second, a naive IM2COL transformation can result in numerous redundant memory accesses. There are several repetitions in the IM2COL patches, which is created by sliding the filters over the input feature map. Depending on the filter size and the stride size, the number of memory access can be  $9\times$  higher on average compared to the number of elements, which indicates that many elements are redundantly accessed multiple times. Our proposed accelerator addresses these issues to improve both performance and energy efficiency.

**Supporting sparsity in CNNs.** Typically, CNNs involve a pruning step that removes unimportant and redundant weights. Pruning leaves many zeros in the trained weights. The resulting sparsity can be exploited to improve performance and energy efficiency. The zeros in the filter and the input feature map can be skipped, which can reduce the number of multiply-accumulates needed and can decrease data movement.

**Techniques for pruning filters.** There are two strategies for pruning: random pruning and structured pruning. The *random pruning* sets a weight to zero if it is below a threshold value [18]. Typically after the pruning step, non-zero weights need to be stored in a compressed sparse format. However, using a sparse format involves indirect accesses and requires extra steps for extracting the non-zero elements and matching indices.

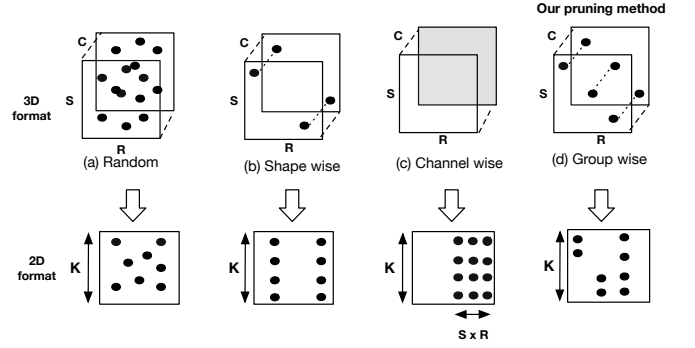


Fig. 4: This figure shows the resulting zeros in the 2-D matrix representation of the filter while pruning the filters at different granularities and their corresponding matrix format. A dark dot indicates that the point is being pruned.

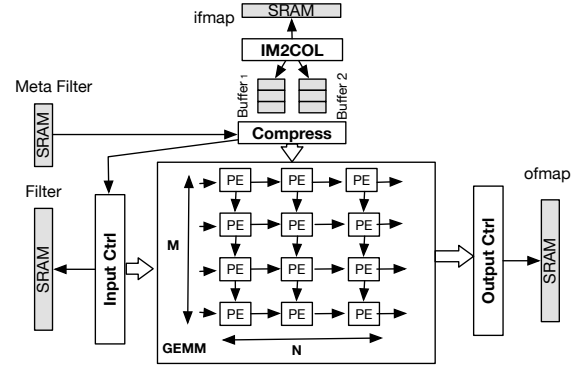


Fig. 5: The overall architecture of our accelerator with the IM2COL unit and a systolic array-based GEMM unit.

In contrast, *structured pruning* address the irregular accesses due to random pruning [25], [27], [49]. Structured pruning removes redundant weights only at well-defined locations or with specific block sizes.

Figure 4 shows pruning at different levels with various pruning methods. The dark points represent pruned weights in the filter. When we convert a 3-D filter to a 2-D representation using the strategy shown in Figure 2(a), resulting zeros in the 2-D matrix is shown in the second row of Figure 4. Random pruning results in an irregular pattern of zeros. A coarse-grained structure (e.g., channel-wise) for pruning can result in a group of zero columns in the 2-D matrix, which is preferable from the computation perspective. However, it can sacrifice network accuracy. A fine-grained structure (e.g., shape-wise) gets closer to the accuracy of random pruning while having a regular structure with zeros.

### III. OUR DESIGN FOR IM2COL AND GEMM BASED CNNs

Our goal is to design a hardware accelerator for inference that provides significant performance and energy benefits for a wide range of CNNs using a GEMM-based formulation of a convolution operation. We propose a hardware unit for the IM2COL transformation that is synergistic and pipelined with the hardware unit for GEMM. The IM2COL unit reads the

input feature map, a 3-D array, and creates a set of linearized patches. The IM2COL unit consists of patch units (PUs) where each PU is responsible for constructing a linear patch. As values are streamed in, the PU constructing the patch will forward redundant elements to neighboring PUs. Once the PU collects all the values in a patch, it forwards in-order partial patches to the GEMM unit. The approach allows the IM2COL unit to read in values from the input feature map once, saving memory accesses. We propose using a tall systolic array-based design for GEMM to maximize the reuse of the result from the IM2COL transformation. It also enables the design to detect zeros in the input feature map and skip columns of the weight matrix of the filter. We propose enhancements to the tall systolic array that allows us to organize it as multiple small systolic arrays for GEMM (see Section III-D), which enables our hardware to adapt to CNN layers with varying dimensions and shapes. Figure 5(a) shows the overall architecture of our accelerator. The two main components are the unit for the IM2COL transformation and the GEMM unit. They are connected by two buffers that allow effective pipelining of the operations between the IM2COL unit and the GEMM unit. Our design focuses on balancing the work by both the IM2COL unit and the GEMM unit.

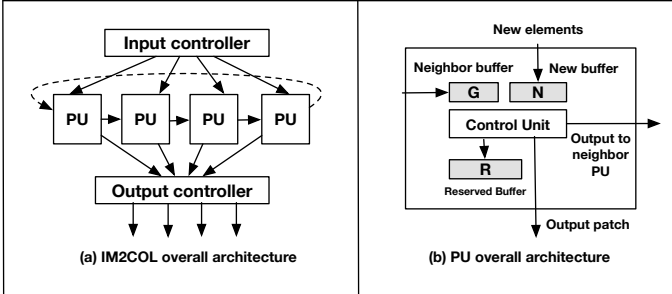


Fig. 6: (a) Overall IM2COL architecture (b) Patch unit internals.

#### A. The IM2COL Unit

The IM2COL transformation creates a 2-D matrix from the 3-D input feature map, which reduces convolution to matrix multiplication. The IM2COL transformation is challenging because it inherits a part of the complexity of convolution, has complex memory access patterns, and results in redundant accesses. We propose a distributed hardware structure that consists of a series of Patch Units (PUs) to both accelerate IM2COL and to minimize the number of accesses to the elements of the input feature map. Each PU is responsible for building one patch at a time. One of our design goals is to read the input feature map only once from SRAM. To accomplish this goal, each patch unit has small local buffers that store some values that will be useful for building future patches. The PUs are connected using a ring network, which allows the PUs to communicate elements locally and minimize accesses to the input feature map in SRAM. Figure 6 shows the overall architecture of our IM2COL unit that consists of three main components: input controller, PUs, and output controller.

The input controller reads the input feature map from SRAM and forwards them to the appropriate PU units. Apart from sending values from the input feature map to the respective PUs, the input controller also maintains some extra metadata for every scheduled patch. This metadata carries information about the position of the current patch. For some convolution layers, stride size is the same as kernel size. In those cases, there is no overlap between the patches. For those scenarios, the input control forwards its output directly to the output controller by skipping the PUs.

Our IM2COL unit has multiple PUs within it. The PUs are the main components of the IM2COL unit for generating patches. Figure 6(b) shows the internals of the PU. Each PU has three buffers: the new buffer, the neighbor buffer, and the reserved buffer. The new buffer (N) maintains the newly fetched element received from the input controller. The neighbor buffer (G) stores the elements received from the neighboring PU. The reserved buffer (R) stores some of the elements previously received at that PU in the previous rounds. We store the row and column indices (*i.e.*, coordinates) along with the value for each element. The control unit within each PU manages the buffer and generates patches. It decides whether an element needs to be forwarded to the neighboring PU and whether it should be maintained in the reserve buffer for future use.

Each patch is identified by a unique identifier (*i.e.*, row and column index of top-left element). The control unit in a PU uses the patch identifier, the filter size, and the stride size to determine which elements need to be (1) fetched from the input feature map, (2) forwarded to the neighboring PUs, and (3) stored in the reserve buffer for future rounds. For example, all elements need to be fetched from the input feature map when a PU processes the first patch in the first round.

All elements that are necessary for adjacent patches in a given round are provided by the neighboring PUs. A PU typically receives  $K^2 - S^2$  elements from the neighboring patches as long as it is not the first patch in a given round, where  $K$  is size of the filter and  $S$  is the stride size. We assign all patches that belong to the same column (*i.e.*, column index of the top-left element) in different rounds to the same PU. Hence, the PUs also stores some elements that may be useful to build patches in subsequent rounds in the reserved buffer. All procedures are performed in the same way for all C channels in the feature map. The output controller organizes patches formed by each PU and manages communications with the GEMM unit. It coordinates double buffering that enables the overlapped execution of the IM2COL unit and the GEMM unit.

Figure 7 illustrates the process of generating the patches using the PUs in our IM2COL unit. For example, PU1 receives four elements (A1, A6, A2, A7) from the input controller and stores it in the new buffer in step 1. Similarly, PU2 receives two new elements (A3, A8). PU2 will receive other elements from the PU1 in subsequent steps (*i.e.*, step 2).

In summary, our hardware IM2COL unit provides two benefits: energy efficiency and performance. Accessing the smaller SRAM and performing integer operations (for computing on row and column indices) consumes significantly less energy



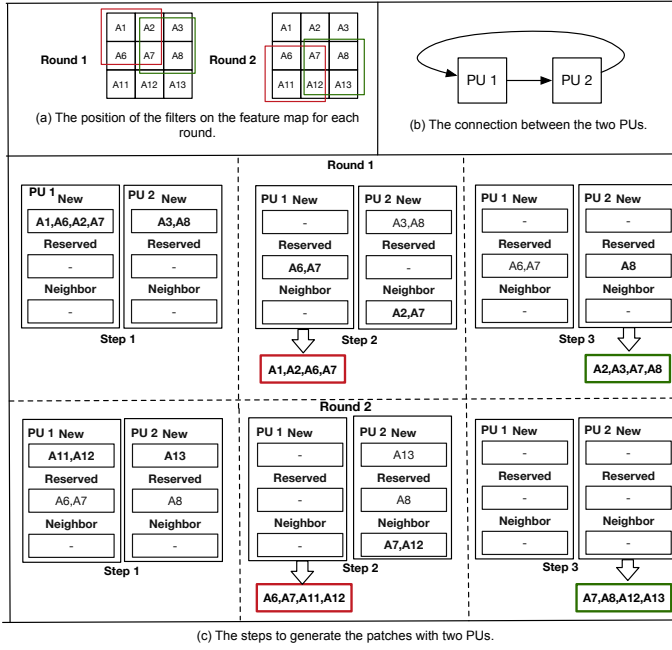


Fig. 7: Illustration of patch generation using the PUs in the IM2COL unit. We show an IM2COL unit with 2 PUs for exposition. (a) The input feature map with one channel. We show the sliding windows used to generate patches with a stride of 1. (b) The two PUs are interconnected by a ring network. (c) There are two rounds. Round 1 corresponds to patches belonging to the first row of sliding windows over the input feature map. Similarly, round 2 corresponds to patches belong to the second row of sliding windows.

than accessing DRAM and large SRAMs. Hence, our design provides significant energy benefits by eliminating redundant accesses, which is needed for the IM2COL transformation otherwise. Further, our distributed collection of PUs unlocks extra parallelism, allowing multiple patches to be built simultaneously by different PUs in the IM2COL unit that boosts performance.

### B. The GEMM Unit

Our hardware unit for accelerating GEMM is a systolic array-based design. Unlike prior proposals that use a square systolic array for GEMM [11], [24], [27], [27], [29], we make a case for a tall systolic array (the height is considerably larger than the width) in our design to maximize data reuse. Figure 8(b) shows our systolic array-based design for GEMM with a tall array. There are two benefits of using a tall systolic array-based design for GEMM. First, one of the inputs of GEMM is generated by the IM2COL unit, and the tall array helps to balance the work done by the GEMM and the IM2COL units. Second, the tall array helps to exploit sparsity in the output of the IM2COL unit to skip zeros and increase performance. As the width of the tall array is smaller than its height, fewer columns from the IM2COL transformation enter the systolic array at any instant of time. Hence, it increases the opportunity for skipping entire rows of inputs with zeros before entering

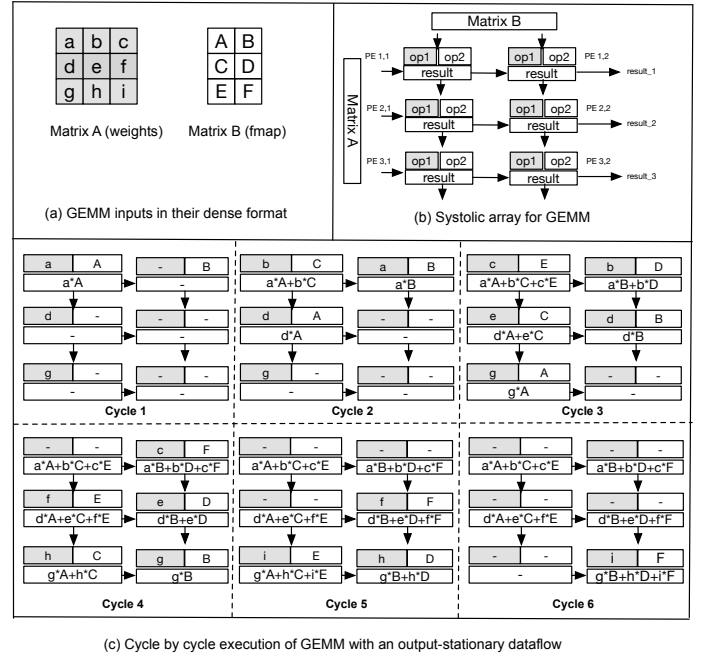


Fig. 8: Illustration of our GEMM unit. (a) Inputs to the GEMM unit. (b) A tall array for the GEMM unit. (c) Illustration of GEMM computation at various steps. We show the current inputs and the partial results computed till a step for each PE. We demonstrate the output-stationary attribute of our design.

the systolic array. The tall array can also be reorganized as multiple GEMM units (see Section III-D).

Our GEMM unit uses an output-stationary dataflow where a given processing element (PE) computes the final result by accumulating the partial products for a particular element of the output. This output-stationary dataflow ensures maximum reuse of the output data. Using a tall array also helps us attain high data reuse for the result of the IM2COL transformation. Figure 8(a) shows the weight matrix from the filter and the output of the IM2COL transformation that forms the input to the GEMM unit. The values of the filter matrix enter the GEMM unit's systolic array from left-to-right. While the result of the IM2COL unit enters the systolic array from top-to-bottom. Figure 8(c) shows the various steps and partial results computed in the GEMM unit. Our design is parameterizable with  $M$  rows and  $N$  columns in the systolic array. In our design, each row handles multiple rows of the filter matrix. Our specific prototype used 128 rows of PEs and 4 columns. Further, each row of the systolic array can be assigned multiple rows of the filter matrix depending on the scheduling mode. The majority of layers in state-of-the-art CNNs have less than 512 rows of the filter matrix in each convolution layer.

Each PE has a single multiply-accumulate (MAC) unit that uses two 16-bit fixed-point inputs and accumulates the result in a 24-bit register. To handle multiple rows of the filter matrix, each PE has  $K$  registers to compute the final result (e.g., in our design, we use  $K = 4$ ). Each PE has three FIFOs. Two FIFOs, one for each arriving inputs. The other FIFO works as

the work queue for the MAC unit. In GEMM, the coordinates of the elements of the two input matrices should match before multiplying the inputs. Our output-stationary dataflow ensures all the partial products produced in a PE belongs to the same output element. Additionally, we ensure that the inputs arrive in the proper order, ensuring that we do not need additional logic to perform index matching inside a PE. Next, we describe how to support sparsities in both inputs without requiring any index matching units inside the PEs.

### C. Handling Sparsity in CNNs

Most CNNs have sparsity in both filters and the input feature map. Figure 13 quantifies the amount of sparsity (percentage of the zeros in the total number of elements) for the commonly used CNNs. We use structured sparsity learning (SSL) [49] as our pruning method that is further enhanced with optimizations to better suit our hardware design (see Section IV). To support sparsity during inference, we propose a custom sparse format to store the filters pruned with our method and design an approach that identifies a block of entries with all zeros in the result of the IM2COL transformation on-the-fly. These techniques enables our accelerator to skip rows and columns with all zeros before entering the systolic array of the GEMM unit. Further, they also allow us to gate the MAC units when an operand is zero. As our designs use a tall systolic array and an output-stationary dataflow, these techniques provides high bandwidth access to the filters and keeps the PEs active.

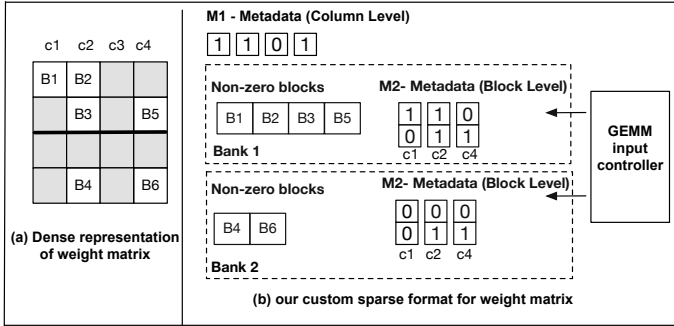


Fig. 9: Our custom sparse format to store filters.

**Our sparse format for filters.** Once the weights for the filters are learned during the training phase, we divide the weights into blocks. The block size is equal to the group size used for pruning, which is a design parameter. Logically, the filter matrix will be 2-D matrix of blocks when viewed in the dense representation. To minimize memory footprint for storing the filters during the inference, we convert them into the sparse representation that is aware of the number of SRAM banks in the design. Our sparse format uses three arrays to store the pruned weights compactly. Figure 9 shows our custom sparse format. We store all non-zero blocks separately in one array (Array A) that is distributed in multiple banks based on the row index of block (*i.e.*, vertical position in the filter matrix). We use two bitmap arrays M1 and M2 to store the metadata. The bitmap array M1 encodes whether a column has any non-zeros

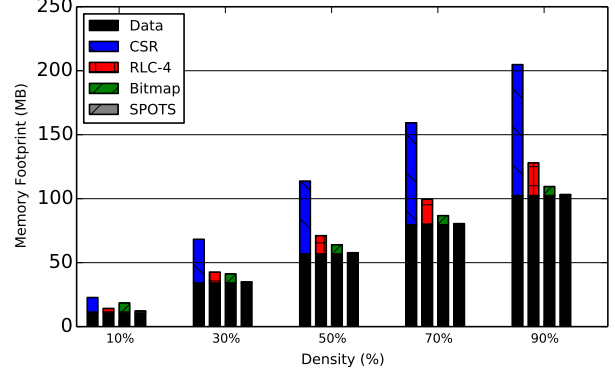


Fig. 10: Comparing our custom sparse format with other state-of-the-art sparse formats. We used a matrix with 1632 rows and 36548 columns. We assume the values are 2 bytes. The last bar shows our sparse format. Our sparse format is independent of the matrix density, and the size of metadata is less than 1 MB across all the density ratios. We compare our sparse format with CSR, RLC-4, and Bitmap in the following order.

in the filter matrix. A zero in the bitmap array M1 indicates an empty column. The bitmap array M2 maintains whether a block in a non-zero column is non-zero. A zero in M2 indicates the corresponding block is zero (*i.e.*, as a block is a collection of values, it implies that all values in the block are zeros). These three arrays of our sparse format (*i.e.*, A, M1, and M2) are distributed across the various banks of the SRAM so that the input controller for the GEMM unit can access them in parallel. Figure 10 compares the memory footprint of our sparse format in contrast to traditional compressed sparse row format and other sparse formats used in prior work. In contrast to them, our sparse format reduces the memory footprint significantly.

**Handling sparsity in the result of the IM2COL transformation.** The *compress* component before the GEMM unit in our accelerator (see Figure 5(a)) identifies a block of zeros in the result of the IM2COL transformation. It creates a bitmap for every block coming out of the IM2COL unit. If all elements in a block in the output of the IM2COL unit are zeros, the bit is set to zero for that block; otherwise, the bit set to one. Subsequently, the input controller of the GEMM unit uses this bitmap to skip blocks with all zeros on-the-fly. We can elide MAC operations when an operand is zero even before entering the systolic array. Further, it is not necessary to stream the column of filters when one detects such a block of zeros. Figure 11 illustrates how the zero columns in the weight matrix and the zero rows in the output of the IM2COL unit are skipped. The  $\star$  marker in Figure 13 indicates the percentage of zeros in the output of the IM2COL transformation that is skipped on-the-fly with this technique. We further reduce energy by gating the MAC units when an operand is zero.

### D. Handling Various CNN Layers/Shapes

CNNs have multiple layers that can be of different shapes and sizes. With a fixed configuration of hardware PEs, they can be underutilized for some layers, shapes and/or sizes. Each filter

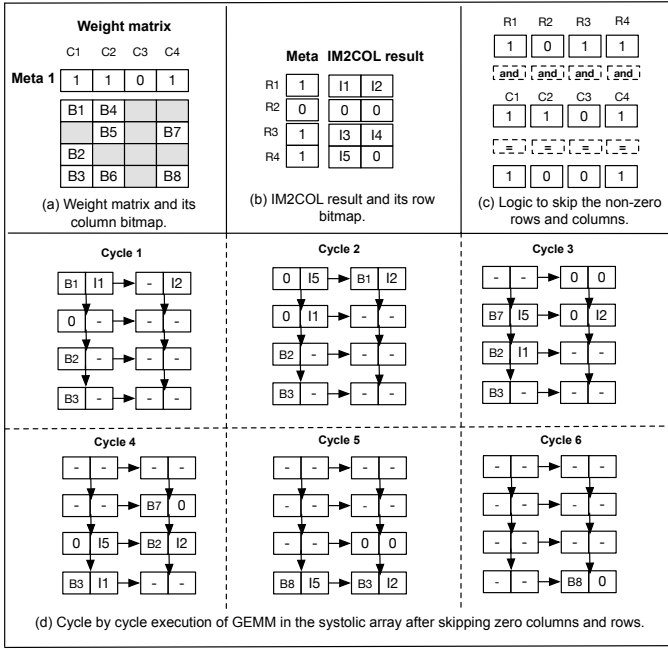


Fig. 11: Illustration of how our design skips rows and columns with all zeros. (a) Weight matrix with the metadata about columns with all zeros. (b) The IM2COL result with the metadata about rows with all zeros. (c) If a row or a column is all zeros, all such rows and columns can be skipped (*i.e.*, and of the row and column metadata). (d) GEMM computation when rows and columns are skipped. For example, the first element of column C4 will be fetched by the first PE in cycle 2 (skipping columns C2 and C3).

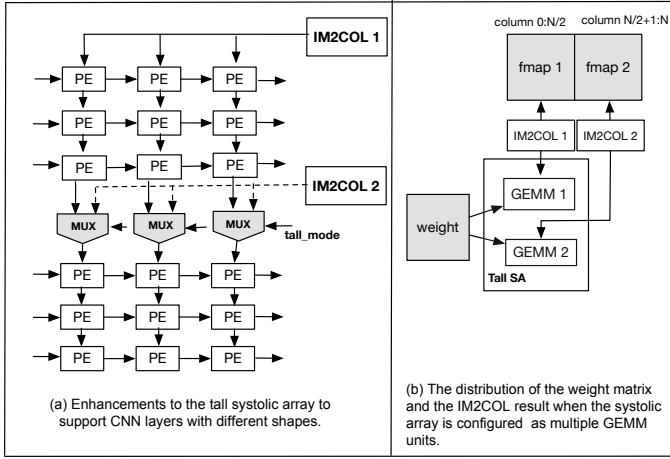


Fig. 12: (a) Enhancements to reorganize the tall systolic array as multiple GEMM units. (b) Illustration of how inputs are distributed in the configuration with multiple GEMM units.

forms a row of the weight matrix that is assigned to a distinct row of the systolic array. In our tall systolic array, when the number of filters is relatively smaller than the systolic array's height (e.g., 128), some PEs will remain unused. To support CNN layers with different attributes, we propose additional enhancements to our design (see Figure 12). Specifically, we organize the PEs in the GEMM unit to be used either as one

tall array or multiple small arrays. Each such configuration has the same number of columns. This enhancement allows our design to be more adaptive to different filter sizes. Figure 12 (a) demonstrates how a tall array can be used as two smaller arrays using the multiplexers. Hence, the PEs now can receive the input either from the PEs above (*i.e.*, it forms a tall array) or can get the input from a different IM2COL unit. These multiplexers can be configured based on the mode register dynamically depending on the structure of a layer. To perform GEMM in the configuration with small arrays, the weight matrix is broadcast to both small systolic arrays. Each such GEMM unit receives the feature map input from their assigned IM2COL units. The two GEMM units compute two independent groups of columns of the final result matrix (*i.e.*, GEMM 1 computes result columns from 0 to  $N/2$ , GEMM computes the columns from  $N/2+1$  to  $N$ ). In our prototype, we have four IM2COL units. The main IM2COL unit is used when the GEMM unit is used in the tall array configuration. Other IM2COL units are smaller in size to reduce the overall area. This dynamic reorganization of the GEMM unit's systolic array coupled with the multiple IM2COL units enables our hardware to support various kinds of CNN layers with different shapes.

**Supporting fully connected layers.** Most CNNs have one or more *fully connected* layers at the end of the network. The inputs to the fully connected layers are the matrix weights learned during the inference and the output feature map resulting from the final pooling or convolutional layer that is flattened to a vector. With a batch size of 1, the computation for a fully connected layer is equivalent to matrix-vector multiplication. By increasing the batch size, we can structure it as a matrix-matrix multiplication operation. As we use a tall array, the batch sizes need not be large (can be as small as 4) when compared to prior work that either have very low PE utilization for fully-connected layers [37] or need batch sizes as large as 16 [11].

**Supporting pooling layers.** The pooling layers help to summarize the features generated by a convolution layer. There are two common types of pooling layers: max pooling and average pooling. Among them, max pooling, which picks the maximum element from a feature covered by the filter, is more common. Similar to convolution layers, the pooling layer has two parameters, filter size and the stride size. Our accelerator supports the pooling layer by adding the pooling operation (e.g., MAX) to the output of the patch units (PUs) in the IM2COL unit.

#### IV. EXPERIMENTAL METHODOLOGY

We created a Verilog implementation of our prototype and synthesized our Verilog implementation of SPOTS using Synopsys Design Compiler with FreePDK 45nm technology [47]. Our design achieves a maximum of 500 MHz frequency. FreePDK 45 does not include SRAM cells. Thus, we separately model the area and power of all the SRAM/DRAM using Cacti 7.0 [9]. Table I provides the parameters of the SPOTS prototype and the area breakdown for different components. We perform a cycle-accurate simulation of the RTL model of SPOTS in

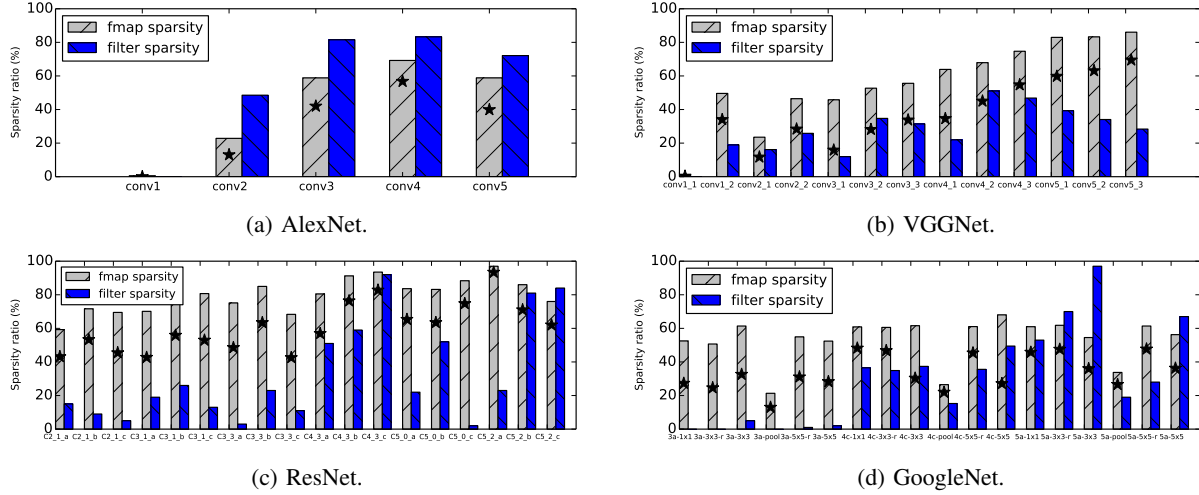


Fig. 13: Sparsity in the filters and input feature maps for AlexNet, VGGNet, ResNet and GoogleNet. The  $\star$  marker indicates the percentage of zeros in the output of the IM2COL transformation that is skipped on-the-fly by our design.

TABLE I: SPOTS design parameters and area.

Unit		Size	Area (mm <sup>2</sup> )
GEMM	#PE units	512	2.048
	Multiplier width	16 bits	
	Accumulator width	24 bits	
	Systolic array configurations	one (128 $\times$ 4)	
	PE's local buffers	four (32 $\times$ 4)	
IM2COL	#PU units	4	1.137
	Reserved buffers	32 KB	
	Other SRAM buffers	2 MB	
On-chip memory	Filter SRAM	1 MB	5.426
	Fmap SRAM	512 KB	
SPOTS total			8.611

TABLE II: The CPU and GPU configurations.

Platform	Configuration
CPU	4 cores, 3 GHz, 32 GB DDR4 (2666 Mhz)
Intel Xeon E5-V3	10 MB Smart Cache, 22nm cell
GPU	3584 cores, Core clock of 1.53 GHz,
Titan X Pascal	24 GB of GDDR5,
	Peak Mem bandwidth of 480 GB/S, 16nm TSMC

Verilog using Verilator [2]. We used the traces from our RTL simulation and estimated the power consumption of our design with Synopsys's PowerPrime tool. During our simulation, we executed each layer at a time. The pruned weights are preprocessed and are provided in our proposed sparse format. For the input feature map, we extracted each layer's data from the models in Caffe. We also developed additional infrastructure to perform fast design space exploration and to collect statistics.

#### CPUs, GPUs, and other ASICs used for our evaluation.

We compare our prototypes with CPUs, GPUs, and other ASICs. We use Caffe [5] to evaluate various CNN architectures on a modern CPU and GPU. The details of the CPU and GPU that we use for the evaluation is shown in Table II. The Caffe framework uses IntelMKL for CPU computation and Nvidia's CUDA library, cuSparse, for the GPU computation. We measured the energy consumption of the XEON CPU using Processor Counter Monitor (PCM) [4], which provides a set

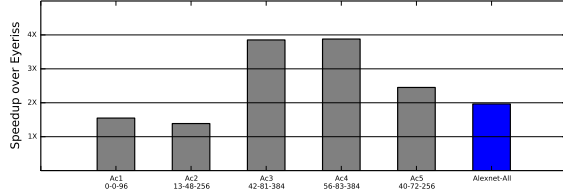
TABLE III: Comparing the top1 and top5 result accuracy for the pruned and the original model.

Model	Dataset	Baseline(%) Top1/Top5 Acc	Our Pruning (%) Top1/Top5 Acc
AlexNet	Imagenet	56.81/79.95	55.25/78.62
VGGNet-16	Imagenet	68.27/88.36	67.18/88.16
GoogleNet	Imagenet	68.92/89.14	66.22/87.53
ResNet-50	Imagenet	77.71/90.66	69.71/89.30

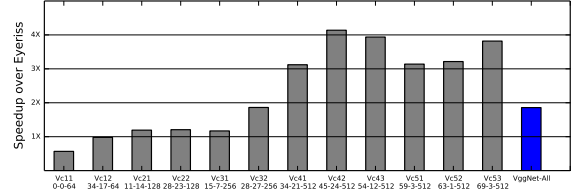
of application programming interfaces (APIs) to monitor the performance and energy metrics of Intel Processors. For GPUs, we measured the power consumption with NVIDIA System Management Interface (Nvidia-smi) [3] that queries the power using the built-in sensors. According to NVIDIA, the reported data is accurate (*i.e.*, within  $\pm 5$  Watt).

**Eyeriss.** Although there are many prior ASICs on accelerating CNN networks, most of them report relative performance numbers, and their designs are not publicly available. We use Eyeriss [10], [11], which is an ASIC designed for accelerating sparse CNNs, to compare against our design. Eyeriss uses a row-stationary (RS) dataflow to maximize data reuse and minimize expensive data movements. Further, data compression and data gating techniques are applied to improve energy efficiency. Eyeriss chip [11] is composed of 168 Processing Elements (PEs) structured as a  $12 \times 14$  array. The PEs are connected with a network-on-chip (NOC) that enables multicast and point-to-point single-cycle data delivery to support the RS dataflow. We measure the performance of Eyeriss using the publicly available simulator [16]. Eyeriss chip is fabricated at 65 nm CMOS and operates at 200 MHz clock frequency. Since we used a different cell technology (*i.e.*, 45 nm) for SPOTS, we assume that the frequency of Eyeriss to be exactly equal to the frequency of SPOTS when we report the execution time. We also configured Eyeriss to use the same number of MAC units and on-chip memory as SPOTS. Additionally, both SPOTS and Eyeriss designs use 16-bit fixed-point inputs.

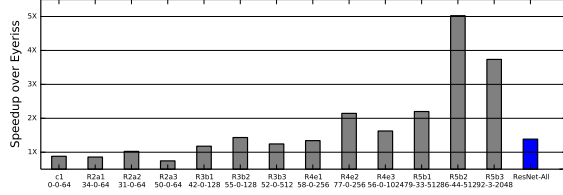




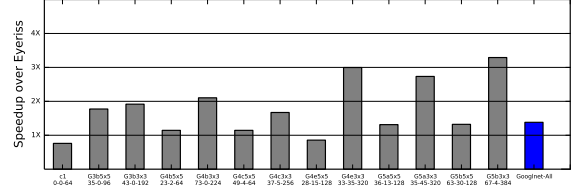
(a) Speedup over Eyeriss for AlexNet.



(b) Speedup over Eyeriss for VGGNet.



(c) Speedup over Eyeriss for ResNet.



(d) Speedup over Eyeriss for GoogleNet.

Fig. 14: Speedup with SPOTS over Eyeriss for four CNNs: AlexNet, VGGNet, ResNet, and GoogleNet.

**CNN architectures and pruning.** We used four widely used CNN architectures: AlexNet [26], VGGNet-16 [44], GoogleNet [48], and Resnet-50 [19] to evaluate our prototype. We refer to VGGNet-16 and ResNet-50 as VGGNet and ResNet, respectively, throughout the paper. These four CNN architectures vary in the number of layers, layer types, and sizes. We used a batch size of one for all of our experiments, which is the standard usage mode for an inference task. We used the input images from the Imagenet [14], a widely used dataset for image classification tasks, to train the networks. We pruned all four networks using the pruning algorithm based on Structure Sparsity Learning (SSL) [49]. SSL is generic and can be applied in different levels, including filters, channels, and shapes. We applied SSL at the shape level. As our hardware exploits sparsity at a much finer granularity than a shape, we optimize SSL by pruning in a more fine-grained fashion. Specifically, we zeroed the weights that are below the threshold in some but not all elements of a shape. This generates zero blocks of a certain size (*i.e.*, the number of filters in the group). Figure 4(d) shows our group-wise pruning. Figure 13 reports the sparsity in the weights and input feature map after pruning for the layers of various CNN architectures. It shows that sparsity varies across both layers and networks. Finally, we retrained the pruned network to regain its accuracy, which is the norm with pruning. Table III reports the top-1 (*i.e.*, the first prediction is the correct result) and top-5 (*i.e.*, the correct result is in the first 5 predicted values) accuracies of the pruned network and the original network. Our pruned networks are within 1%-2% accuracy of the original model without pruning.

## V. EVALUATION

We demonstrate the performance and energy efficiency of our prototype, SPOTS, in comparison to Eyeriss and CPU/GPU implementations.

**Performance of SPOTS when compared to Eyeriss.** Figure 14 reports the speedup of SPOTS relative to Eyeriss for all four CNN architectures. The sparsity ratio for the input

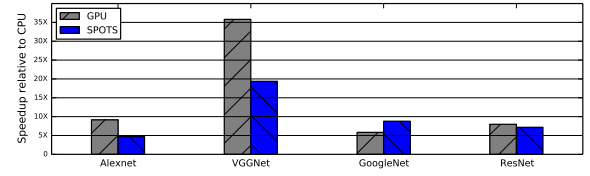


Fig. 15: Speedup with SPOTS and GPU implementations over the CPU implementation as the baseline.

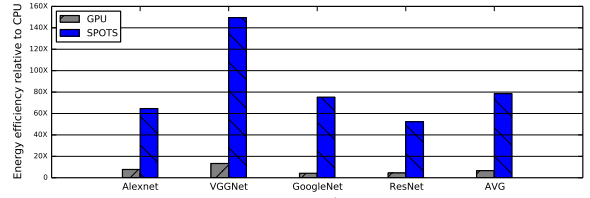


Fig. 16: Energy efficiency of SPOTS and GPU implementations compared to a CPU baseline.

feature map, filters, and the number of filters are shown below each layer. The layers are sorted for each CNN architecture based on where they appear in the network (top, middle, or bottom). Figure 14(a) reports the speedup for all layers in AlexNet. On average, SPOTS is almost  $2\times$  faster than Eyeriss. SPOTS is almost  $4\times$  faster than Eyeriss for the layers in the middle of the network because those layers have more sparsity in the input feature map and the filters when compared to the top or bottom layers. SPOTS detects zeros on-the-fly in the input feature map compared to Eyeriss, which is the reason for the speedup.

Figure 14(b) reports that SPOTS has  $1.85\times$  faster than Eyeriss on average for the 12 layers in VGGNet. Similar to AlexNet, SPOTS achieves higher speedup in layers with more sparsity. SPOTS is slightly worse than Eyeriss for the first two layers, where the number of filters is relatively smaller than the width of the input feature map. Figure 14(c) shows the

speedup of SPOTS over Eyeriss for all the convolution layers in ResNet. SPOTS is  $1.38\times$  faster than Eyeriss on average for all the convolution layers in ResNet. SPOTS is more than  $8\times$  faster than Eyeriss for some layers. Our design performs slightly worse or similar to Eyeriss for the first eight layers in ResNet because the first few layers in ResNet have a small number of filters per layer. Hence, PEs are underutilized compared to layers in the middle or at the end of the network. Figure 14(d) shows that SPOTS is  $1.38\times$  faster than Eyeriss for GoogleNet. In contrast to other CNN architectures, GoogleNet has a few convolutional layers at the beginning with a small number of filters. The PEs are not effectively utilized with SPOTS resulting in relatively lower speedups compared to other CNN architectures.

**Performance comparison with CPUs and GPUs.** We evaluate the performance and energy efficiency of SPOTS in comparison to execution with CPUs and GPUs. Figure 15 reports the speedup of SPOTS for the convolution layers over the CPU implementation. SPOTS has  $5\times$ ,  $20\times$ ,  $6\times$  and  $8\times$  speedup over the CPU implementations using Intel MKL for AlexNet, VGGNet, GoogleNet, and ResNet, respectively. SPOTS attains this speedup while operating at a frequency almost  $6\times$  less than the CPU. Figure 15 also reports the speedup of GPUs for the convolution layers over the CPU implementation. Compared to GPUs, SPOTS is about  $2\times$  slower than GPU for AlexNet and VGGNet, while performs slightly better or similar to GPU for GoogleNet and ResNet. The GPU used for this evaluation has  $7\times$  more MAC units than SPOTS and it operates at a frequency nearly  $3\times$  higher than SPOTS. As we use a structured pruning approach, it also helps the GPU implementation to attain better performance.

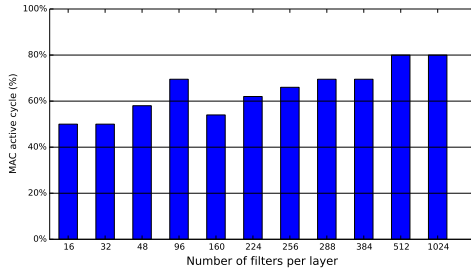


Fig. 17: MAC utilization (*i.e.*, active cycles) for different filter sizes.

**Energy efficiency compared to CPUs and GPUs.** We also evaluate the energy efficiency of SPOTS in comparison to CPUs and GPUs. While GPUs are powerful with their abundant computations and memory resources, they are power hungry. Figure 16 demonstrates the energy efficiency of SPOTS and GPU implementations when compared to a CPU baseline. for four CNNs. We include the energy of off-chip memory accesses in this data. Our accelerator consumes  $78\times$  and  $12\times$  lesser energy than a CPU and a GPU implementation, respectively.

**Sensitivity to shapes of various layers.** Widely used CNN networks vary in the depth and the number of filters used in each layer. Even within a CNN, the layer shape and filter

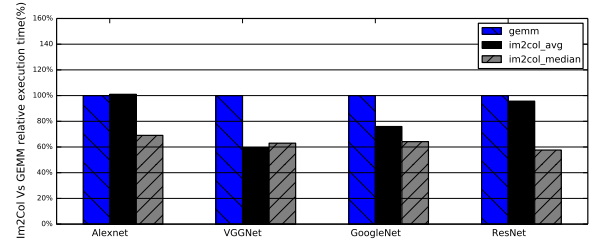


Fig. 18: Fraction of the work performed by the IM2COL unit when compared to GEMM (*i.e.*, GEMM bar is 100%). We report the average and the median for the IM2COL’s work. When the mean exceeds the median, there will be instances where the IM2COL does significantly more work compared to GEMM for some layers.

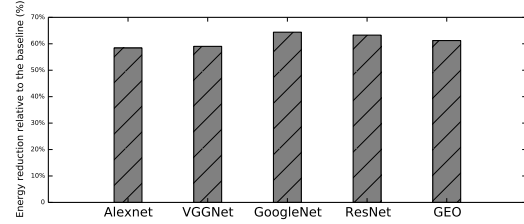


Fig. 19: The reduction in energy consumption for the IM2COL unit of SPOTS over the baseline design.

sizes can vary significantly. SPOTS provides flexibility to use the GEMM unit as a tall systolic array or as multiple small systolic arrays to adapt to various shapes and filter sizes. When the filters are small (*e.g.*, less than 128), the GEMM unit is configured as multiple small systolic arrays, which use different IM2COL units. All PEs in the systolic array are active 100% of the time for all filter sizes other than 16. Figure 17 shows the utilization of the multiply-accumulate units in the PEs of the systolic array (*i.e.*, active cycles) when the layer has a specified number of filters (*i.e.*, x-axis reports the size of the filter). When the filter size increases, we assign more rows to a PE, which can fetch up to four elements per read operation. Hence, there are more opportunities to keep the multiply-accumulate units in the PE active (*i.e.*, almost 80% active cycles).

**Amount of work performed by IM2COL and GEMM units in SPOTS.** As the IM2COL and the GEMM units are pipelined in SPOTS, ideally, we want the the work performed by the IM2COL unit and the GEMM unit to be balanced. Figure 18 shows the relative percentage of cycles where the IM2COL and GEMM units are active relative to the GEMM unit for the four CNN architectures. As we report the active cycles relative to the GEMM unit, the bar for the GEMM unit is 100%. The average work performed by the IM2COL unit and the GEMM unit are almost similar for AlexNet and ResNet (*i.e.*, the work is balanced). In contrast, GEMM dominates the total work in VGGNet. This data suggests that adding more PE’s to the GEMM unit may improve the overall execution time for VGGNet. As the IM2COL unit is inactive due to low bandwidth with AlexNet and ResNext, adding more PEs without increasing the bandwidth will not improve performance.

TABLE IV: Qualitative comparison of SPOTS with or it some of the prior works.

Accelerator	Supports sparsity				Supports pruned network	Adaptive to different layer shapes	Supports FC	Supports Pooling
	Feature map	Weight	Gate zero	Skip zero				
Eyeriss [11]	✓	✗	✓	✗	✗	✗	✓	✗
Cnvlutin [7]	✓	✗	✓	✓	✗	✗	✓	✗
CambriconS [53]	✓	✓	✗	✓	✓(structured)	✗	✓	✗
SCNN [37]	✓	✓	✓	✓	✓(random)	✗	✓	✓
Column combining [27]	✗	✓	✗	✓	✓(structured)	✗	✓	✗
SIGMA [38]	✓	✓	✗	✓	✓(random)	✓	✓	✗
SPOTS (this work)	✓	✓	✓	✓	✓structured	✓	✓	✓

### Energy efficiency from data reuse in the IM2COL unit.

One of the key ideas in the IM2COL’s patch unit is to read the input feature map only once from the SRAM and reuse the data with the help of local buffers. Figure 19 reports the percentage decrease in energy consumed by using local buffers to reuse the data in the patch units compared to a naive version of IM2COL that uses SRAMs multiple times without data reuse. On average, the mechanisms that we added to reuse the input feature map in the patch units result in the IM2COL unit consume 60% less energy when compared to the IM2COL unit without such reuse.

## VI. RELATED WORK

There is a large body of literature on using custom hardware accelerators to improve the performance and energy efficiency of neural networks [6], [7], [11], [12], [12], [17], [23], [37], [39], [41], [42], [51]. Table IV qualitatively compares SPOTS with the closely related prior work on various dimensions.

**Support for sparse inputs.** Prior work has improved energy efficiency by supporting sparse inputs during inference. Cnvlutin [7] exploits sparsity in the input feature map to skip multiplication operations and to avoid data movement with zero elements. CambriconX [51] supports sparsity in the weights. Similar to our work, SCNN [37] and CambriconS [53] support sparsity in both the feature map and the weights to improve energy efficiency and performance. Prior work also uses data gating techniques to reduce the power consumption when the operands are zeros [11], [39]. While this technique is effective in reducing power consumption, it does not reduce the number of effective operations. Similar to SPOTS, prior hardware designs have developed techniques to skip zeros collectively to minimize data movement across various memory hierarchies [17], [33], [37].

**Support for CNNs with layers of varying shapes.** Often, hardware designs are primarily customized for one type of computation. Most prior prototypes do not support all types of layers in CNN, such as pooling layers [8], [27]. EIE [17] is intended for the fully connected layers in CNNs. It stores the input feature map and filters in a compressed format and passes only non-zero operands to the multipliers. In contrast, SCNN [37] and Eyeriss [10], [11] primarily focus on the convolution layers. Hence, they can underperform for the fully-connected layers. SCNN can achieve 25% of peak throughput when performing the fully connected CNN layers. Similarly, Eyeriss provides significant energy gains only when batch sizes are larger than 16.

**Systolic array designs for CNNs.** Recent work [20], [27] uses a preprocessing step (i.e., column combining) to pack a sparse CNN into a denser form before passing the inputs to a systolic array for GEMM. It is unclear how to prepare input feature maps for matrix multiplication. It will not provide benefits when there is abundant sparsity in the input feature map. Our group-wise pruning provides higher accuracy than the column combining method. Simultaneous multithreaded systolic array (SMT-SA) [43] addresses the under utilization and load imbalance introduced by random pruning of the weights in a CNN. Similar to SPOTS, recent work [31] utilizes a structured pruning accompanied with a novel data format called density-bound block (DBB) better to map the sparse inputs to the systolic architecture. None of the prior work designs the IM2COL transformation to use matrix multiplication with a convolution and utilizes the sparsity in the input feature map.

**Flexible interconnects.** Flexible interconnects between the processing elements can help adapt to various input and filter sizes [30], [38]. Maeri [30] enables a flexible dataflow mapping over DNN accelerators using a tree-based reconfigurable interconnects network. A downside of MAERI is that it does not handle input feature map sparsity. Similarly, FlexFlow [32] develops a flexible dataflow architecture that exploits different types of parallelism along with different CNN workloads. In contrast to them, SPOTS uses a regular interconnect network between the PEs. SIGMA [38] is another recent work that proposes a flexible non-blocking interconnect to achieve high compute utilization across layers of varying shapes. SIGMA is primarily optimized for high precision inputs during the training phase. Besides, they solely focus on the GEMM and do not study the IM2COL transformation and support other types of layers in a CNN.

**Other accelerators.** Recent work has explored the design space of hardware accelerators for optimal dataflow and scheduling schemes for neural networks [15], [16], [28], [36], [50]. Beyond sparse convolution, custom hardware to accelerate sparse matrix-matrix multiplication with very sparse matrices (i.e., density below 1%) have also been explored [21], [22], [35], [45], [46], [52]. To improve the efficiency of an inference task, recent work has also decomposed multiplications in a neural network down to the bit level [6], [41]. The bit-level decomposition increases the ability to detect and skip computation with zeros.

## VII. CONCLUSION

This paper proposes SPOTS, a hardware accelerator for sparse CNNs with a matrix multiplication formulation of a convolution using the IM2COL transformation. The hardware IM2COL unit reads the input feature map only once, reuses the data, and executes in parallel with a tall systolic array for the GEMM unit. We add the flexibility to the systolic array that enables it to adapt to CNN layers of varying sizes. SPOTS supports sparsity both in the input feature map and the filters. SPOTS is faster and more energy efficient than state-of-the-art accelerators, CPU, and GPU implementations for sparse CNNs.

## REFERENCES

- [1] [Online]. Available: <https://aws.amazon.com/machine-learning/inferential/>
- [2] [Online]. Available: <https://www.veripool.org/verilator/>
- [3] "Nvidia system management interface (nvdi-smi)." [Online]. Available: <https://developer.download.nvidia.com/compute/DCGM/docs/nvidia-smi-367.38.pdf>
- [4] "Processor counter monitor (pcm)." [Online]. Available: <https://github.com/opcm/pcm>
- [5] 2021, pp. 248–255. [Online]. Available: <http://caffe.berkeleyvision.org>
- [6] J. Albericio, A. Delmás, P. Judd, S. Sharify, G. O'Leary, R. Genov, and A. Moshovos, "Bit-pragmatic deep neural network computing," in *2017 50th Annual IEEE/ACM International Symposium on Microarchitecture (MICRO)*, 2017, pp. 382–394.
- [7] J. Albericio, P. Judd, T. Hetherington, T. Aamodt, N. E. Jerger, and A. Moshovos, "Cnvlutin: Ineffectual-neuron-free deep neural network computing," *SIGARCH Comput. Archit. News*, vol. 44, no. 3, p. 1–13, Jun. 2016. [Online]. Available: <https://doi.org/10.1145/3007787.3001138>
- [8] B. Asgari, R. Hadidi, H. Kim, and S. Yalamanchili, "Eridanus: Efficiently running inference of dnns using systolic arrays," *IEEE Micro*, vol. 39, no. 5, pp. 46–54, 2019.
- [9] R. Balasubramanian, A. B. Kahng, N. Muralimanohar, A. Shafiee, and V. Srinivas, "Cacti 7: New tools for interconnect exploration in innovative off-chip memories," *ACM Trans. Archit. Code Optim.*, vol. 14, no. 2, Jun. 2017. [Online]. Available: <https://doi.org/10.1145/3085572>
- [10] Y.-H. Chen, J. Emer, and V. Sze, "Eyeriss: A spatial architecture for energy-efficient dataflow for convolutional neural networks," in *2016 ACM/IEEE 43rd Annual International Symposium on Computer Architecture (ISCA)*, 2016, pp. 367–379.
- [11] Y.-H. Chen, T. Krishna, J. S. Emer, and V. Sze, "Eyeriss: An energy-efficient reconfigurable accelerator for deep convolutional neural networks," *IEEE Journal of Solid-State Circuits*, vol. 52, no. 1, pp. 127–138, 2017.
- [12] Y. Chen, T. Luo, S. Liu, S. Zhang, L. He, J. Wang, L. Li, T. Chen, Z. Xu, N. Sun, and O. Temam, "Dadiannao: A machine-learning super-computer," in *2014 47th Annual IEEE/ACM International Symposium on Microarchitecture*, 2014, pp. 609–622.
- [13] R. Collobert, J. Weston, L. Bottou, M. Karlen, K. Kavukcuoglu, and P. Kuksa, "Natural language processing (almost) from scratch," *J. Mach. Learn. Res.*, vol. 12, no. null, p. 2493–2537, Nov. 2011.
- [14] J. Deng, W. Dong, R. Socher, L.-J. Li, K. Li, and L. Fei-Fei, "Imagenet: A large-scale hierarchical image database," in *2009 IEEE Conference on Computer Vision and Pattern Recognition*, 2009, pp. 248–255.
- [15] M. Gao, J. Pu, X. Yang, M. Horowitz, and C. Kozyrakis, "Tetris: Scalable and efficient neural network acceleration with 3d memory," *SIGARCH Comput. Archit. News*, vol. 45, no. 1, p. 751–764, Apr. 2017. [Online]. Available: <https://doi.org/10.1145/3093337.3037702>
- [16] M. Gao, X. Yang, J. Pu, M. Horowitz, and C. Kozyrakis, "Tangram: Optimized coarse-grained dataflow for scalable nn accelerators," in *Proceedings of the Twenty-Fourth International Conference on Architectural Support for Programming Languages and Operating Systems*, ser. ASPLOS '19. New York, NY, USA: Association for Computing Machinery, 2019, p. 807–820. [Online]. Available: <https://doi.org/10.1145/3297858.3304014>
- [17] S. Han, X. Liu, H. Mao, J. Pu, A. Pedram, M. A. Horowitz, and W. J. Dally, "Eie: Efficient inference engine on compressed deep neural network," in *2016 ACM/IEEE 43rd Annual International Symposium on Computer Architecture (ISCA)*, 2016, pp. 243–254.
- [18] S. Han, H. Mao, and W. J. Dally, "Deep compression: Compressing deep neural networks with pruning, trained quantization and huffman coding," 2016.
- [19] K. He, X. Zhang, S. Ren, and J. Sun, "Deep residual learning for image recognition," in *2016 IEEE Conference on Computer Vision and Pattern Recognition (CVPR)*, 2016, pp. 770–778.
- [20] X. He, S. Pal, A. Amarnath, S. Feng, D.-H. Park, A. Rovinski, H. Ye, Y. Chen, R. Dreslinski, and T. Mudge, "Sparse-tpu: Adapting systolic arrays for sparse matrices," in *Proceedings of the 34th ACM International Conference on Supercomputing*, ser. ICS '20. New York, NY, USA: Association for Computing Machinery, 2020. [Online]. Available: <https://doi.org/10.1145/3392717.3392751>
- [21] K. Hegde, H. Asghari-Moghaddam, M. Pellauer, N. Crago, A. Jaleel, E. Solomonik, J. Emer, and C. W. Fletcher, "Extensor: An accelerator for sparse tensor algebra," in *Proceedings of the 52nd Annual IEEE/ACM International Symposium on Microarchitecture*, ser. MICRO '52. New York, NY, USA: Association for Computing Machinery, 2019, p. 319–333. [Online]. Available: <https://doi.org/10.1145/3352460.3358275>
- [22] R. Hojabr, A. Sedaghati, A. Sharifian, A. Khonsari, and A. Shriraman, "Spaghetti: Streaming accelerators for highly sparse gemm on fpgas," in *2021 IEEE International Symposium on High-Performance Computer Architecture (HPCA)*, 2021, pp. 84–96.
- [23] C.-T. Huang, Y.-C. Ding, H.-C. Wang, C.-W. Weng, K.-P. Lin, L.-W. Wang, and L.-D. Chen, "Ecnn: A block-based and highly-parallel cnn accelerator for edge inference," in *Proceedings of the 52nd Annual IEEE/ACM International Symposium on Microarchitecture*, ser. MICRO '52. New York, NY, USA: Association for Computing Machinery, 2019, p. 182–195. [Online]. Available: <https://doi.org/10.1145/3352460.3358263>
- [24] N. P. Jouppi, C. Young, N. Patil, D. Patterson, G. Agrawal, R. Bajwa, S. Bates, S. Bhatia, N. Boden, A. Borchers, R. Boyle, P.-I. Cantin, C. Chao, C. Clark, J. Coriell, M. Daley, M. Dau, J. Dean, B. Gelb, T. V. Ghaemmaghami, R. Gottipati, W. Gulland, R. Hagmann, C. R. Ho, D. Hogberg, J. Hu, R. Hundt, D. Hurt, J. Ibarz, A. Jaffey, A. Jaworski, A. Kaplan, H. Khaitan, D. Killebrew, A. Koch, N. Kumar, S. Lacy, J. Laudon, J. Law, D. Le, C. Leary, Z. Liu, K. Lucke, A. Lundin, G. MacKean, A. Maggiore, M. Mahony, K. Miller, R. Nagarajan, R. Narayanaswami, R. Ni, K. Nix, T. Norrie, M. Omernick, N. Penukonda, A. Phelps, J. Ross, M. Ross, A. Salek, E. Samadiani, C. Severn, G. Sizikov, M. Snellman, J. Souter, D. Steinberg, A. Swing, M. Tan, G. Thorson, B. Tian, H. Toma, E. Tuttle, V. Vasudevan, C. Walter, W. Wang, E. Wilcox, and D. H. Yoon, "In-datacenter performance analysis of a tensor processing unit," in *Proceedings of the 44th Annual International Symposium on Computer Architecture*, ser. ISCA '17. New York, NY, USA: Association for Computing Machinery, 2017, p. 1–12. [Online]. Available: <https://doi.org/10.1145/3079856.3080246>
- [25] H.-J. Kang, "Accelerator-aware pruning for convolutional neural networks," *IEEE Transactions on Circuits and Systems for Video Technology*, vol. 30, no. 7, pp. 2093–2103, 2020.
- [26] A. Krizhevsky, I. Sutskever, and G. E. Hinton, "Imagenet classification with deep convolutional neural networks," *Commun. ACM*, vol. 60, no. 6, p. 84–90, May 2017. [Online]. Available: <https://doi.org/10.1145/3065386>
- [27] H. Kung, B. McDanel, and S. Q. Zhang, "Packing sparse convolutional neural networks for efficient systolic array implementations: Column combining under joint optimization," in *Proceedings of the Twenty-Fourth International Conference on Architectural Support for Programming Languages and Operating Systems*, ser. ASPLOS '19. New York, NY, USA: Association for Computing Machinery, 2019, p. 821–834. [Online]. Available: <https://doi.org/10.1145/3297858.3304028>
- [28] H. Kwon, P. Chatarasi, M. Pellauer, A. Parashar, V. Sarkar, and T. Krishna, "Understanding reuse, performance, and hardware cost of dnn dataflow: A data-centric approach," in *Proceedings of the 52nd Annual IEEE/ACM International Symposium on Microarchitecture*, ser. MICRO '52. New York, NY, USA: Association for Computing Machinery, 2019, p. 754–768. [Online]. Available: <https://doi.org/10.1145/3352460.3358252>
- [29] H. Kwon, L. Lai, M. Pellauer, T. Krishna, Y.-H. Chen, and V. Chandra, "Heterogeneous dataflow accelerators for multi-dnn workloads," 2019.
- [30] H. Kwon, A. Samajdar, and T. Krishna, "Maeri: Enabling flexible dataflow mapping over dnn accelerators via reconfigurable interconnects," *SIGPLAN Not.*, vol. 53, no. 2, p. 461–475, Mar. 2018. [Online]. Available: <https://doi.org/10.1145/3296957.3173176>
- [31] Z.-G. Liu, P. N. Whatmough, and M. Mattina, "Systolic tensor array: An efficient structured-sparse gemm accelerator for mobile cnn inference," *IEEE Computer Architecture Letters*, vol. 19, no. 1, pp. 34–37, 2020.



- [32] W. Lu, G. Yan, J. Li, S. Gong, Y. Han, and X. Li, "Flexflow: A flexible dataflow accelerator architecture for convolutional neural networks," in *2017 IEEE International Symposium on High Performance Computer Architecture (HPCA)*, 2017, pp. 553–564.
- [33] H. Mo, L. Liu, W. Hu, W. Zhu, Q. Li, A. Li, S. Yin, J. Chen, X. Jiang, and S. Wei, "Tfe: Energy-efficient transferred filter-based engine to compress and accelerate convolutional neural networks," in *2020 53rd Annual IEEE/ACM International Symposium on Microarchitecture (MICRO)*, 2020, pp. 751–765.
- [34] E. Nurvitadhi, G. Venkatesh, J. Sim, D. Marr, R. Huang, J. Ong Gee Hock, Y. T. Liew, K. Srivatsan, D. Moss, S. Subhaschandra, and G. Boudoukh, "Can fpgas beat gpus in accelerating next-generation deep neural networks?" in *Proceedings of the 2017 ACM/SIGDA International Symposium on Field-Programmable Gate Arrays*, ser. FPGA '17. New York, NY, USA: Association for Computing Machinery, 2017, p. 5–14. [Online]. Available: <https://doi.org/10.1145/3020078.3021740>
- [35] S. Pal, J. Beaumont, D. Park, A. Amarnath, S. Feng, C. Chakrabarti, H. Kim, D. Blaauw, T. Mudge, and R. Dreslinski, "Outerspace: An outer product based sparse matrix multiplication accelerator," in *HPCA*, Feb 2018, pp. 724–736.
- [36] A. Parashar, P. Raina, Y. S. Shao, Y.-H. Chen, V. A. Ying, A. Mukkara, R. Venkatesan, B. Khailany, S. W. Keckler, and J. Emer, "Timeloop: A systematic approach to dnn accelerator evaluation," in *2019 IEEE International Symposium on Performance Analysis of Systems and Software (ISPASS)*, 2019, pp. 304–315.
- [37] A. Parashar, M. Rhu, A. Mukkara, A. Puglielli, R. Venkatesan, B. Khailany, J. Emer, S. W. Keckler, and W. J. Dally, "Scnn: An accelerator for compressed-sparse convolutional neural networks," in *2017 ACM/IEEE 44th Annual International Symposium on Computer Architecture (ISCA)*, 2017, pp. 27–40.
- [38] E. Qin, A. Samajdar, H. Kwon, V. Nadella, S. Srinivasan, D. Das, B. Kaul, and T. Krishna, "Sigma: A sparse and irregular gemm accelerator with flexible interconnects for dnn training," in *2020 IEEE International Symposium on High Performance Computer Architecture (HPCA)*, 2020, pp. 58–70.
- [39] B. Reagen, P. Whatmough, R. Adolf, S. Rama, H. Lee, S. K. Lee, J. M. Hernández-Lobato, G.-Y. Wei, and D. Brooks, "Minerva: Enabling low-power, highly-accurate deep neural network accelerators," in *Proceedings of the 43rd International Symposium on Computer Architecture*, ser. ISCA '16. IEEE Press, 2016, p. 267–278. [Online]. Available: <https://doi.org/10.1109/ISCA.2016.32>
- [40] D. B. Schwartz, R. E. Howard, and W. E. Hubbard, "A programmable analog neural network chip," *IEEE Journal of Solid-State Circuits*, vol. 24, no. 2, pp. 313–319, 1989.
- [41] S. Sharify, A. D. Lascorz, M. Mahmoud, M. Nikolic, K. Siu, D. M.
- [49] W. Wen, C. Wu, Y. Wang, Y. Chen, and H. Li, "Learning structured sparsity in deep neural networks," in *Proceedings of the 30th International*
- Stuart, Z. Poulos, and A. Moshovos, "Laconic deep learning inference acceleration," in *2019 ACM/IEEE 46th Annual International Symposium on Computer Architecture (ISCA)*, 2019, pp. 304–317.
- [42] H. Sharma, J. Park, D. Mahajan, E. Amaro, J. K. Kim, C. Shao, A. Mishra, and H. Esmaeilzadeh, "From high-level deep neural models to fpgas," in *2016 49th Annual IEEE/ACM International Symposium on Microarchitecture (MICRO)*, 2016, pp. 1–12.
- [43] G. Shomron, T. Horowitz, and U. Weiser, "Smt-sa: Simultaneous multithreading in systolic arrays," *IEEE Computer Architecture Letters*, vol. 18, no. 2, pp. 99–102, 2019.
- [44] K. Simonyan and A. Zisserman, "Very deep convolutional networks for large-scale image recognition," 2015.
- [45] M. Soltaniyeh, R. P. Martin, and S. Nagarakatte, "Synergistic cpu-fpga acceleration of sparse linear algebra," 2020.
- [46] N. Srivastava, H. Jin, J. Liu, D. Albonese, and Z. Zhang, "Matraptor: A sparse-sparse matrix multiplication accelerator based on row-wise product," in *MICRO*, 2020, pp. 766–780.
- [47] J. E. Stine, I. Castellanos, M. Wood, J. Henson, F. Love, W. R. Davis, P. D. Franzon, M. Bucher, S. Basavarajaiah, J. Oh, and R. Jenkal, "Freeptk: An open-source variation-aware design kit," in *2007 IEEE International Conference on Microelectronic Systems Education (MSE'07)*, 2007, pp. 173–174.
- [48] C. Szegedy, W. Liu, Y. Jia, P. Sermanet, S. Reed, D. Anguelov, D. Erhan, V. Vanhoucke, and A. Rabinovich, "Going deeper with convolutions," in *2015 IEEE Conference on Computer Vision and Pattern Recognition (CVPR)*, 2015, pp. 1–9. *Conference on Neural Information Processing Systems*, ser. NIPS'16. Red Hook, NY, USA: Curran Associates Inc., 2016, p. 2082–2090.
- [50] X. Yang, M. Gao, Q. Liu, J. Setter, J. Pu, A. Nayak, S. Bell, K. Cao, H. Ha, P. Raina, C. Kozyrakis, and M. Horowitz, "Interstellar: Using halide's scheduling language to analyze dnn accelerators," in *Proceedings of the Twenty-Fifth International Conference on Architectural Support for Programming Languages and Operating Systems*, ser. ASPLOS '20. New York, NY, USA: Association for Computing Machinery, 2020, p. 369–383. [Online]. Available: <https://doi.org/10.1145/3373376.3378514>
- [51] S. Zhang, Z. Du, L. Zhang, H. Lan, S. Liu, L. Li, Q. Guo, T. Chen, and Y. Chen, "Cambricon-x: An accelerator for sparse neural networks," in *2016 49th Annual IEEE/ACM International Symposium on Microarchitecture (MICRO)*, 2016, pp. 1–12.
- [52] Z. Zhang, H. Wang, S. Han, and W. J. Dally, "Sparch: Efficient architecture for sparse matrix multiplication," in *HPCA*, 2020.
- [53] X. Zhou, Z. Du, Q. Guo, S. Liu, C. Liu, C. Wang, X. Zhou, L. Li, T. Chen, and Y. Chen, "Cambricon-s: Addressing irregularity in sparse neural networks through a cooperative software/hardware approach," in *2018 51st Annual IEEE/ACM International Symposium on Microarchitecture (MICRO)*, 2018, pp. 15–28.